

# Magnetic shielding of walls from the unmagnetized ion beam in a Hall thruster

Cite as: Appl. Phys. Lett. **102**, 023509 (2013); <https://doi.org/10.1063/1.4776192>

Submitted: 04 August 2012 . Accepted: 20 December 2012 . Published Online: 17 January 2013

Ioannis G. Mikellides, Ira Katz, Richard R. Hofer, Dan M. Goebel, et al.



View Online



Export Citation



CrossMark

## ARTICLES YOU MAY BE INTERESTED IN

[Magnetic shielding of a laboratory Hall thruster. I. Theory and validation](#)

Journal of Applied Physics **115**, 043303 (2014); <https://doi.org/10.1063/1.4862313>

[Magnetic shielding of a laboratory Hall thruster. II. Experiments](#)

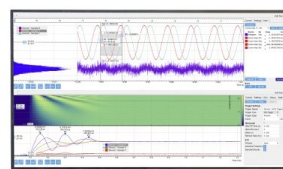
Journal of Applied Physics **115**, 043304 (2014); <https://doi.org/10.1063/1.4862314>

[Magnetic shielding of the channel walls in a Hall plasma accelerator](#)

Physics of Plasmas **18**, 033501 (2011); <https://doi.org/10.1063/1.3551583>

Challenge us.

What are your needs for periodic signal detection?



Zurich Instruments



# Magnetic shielding of walls from the unmagnetized ion beam in a Hall thruster

Ioannis G. Mikellides,<sup>a)</sup> Ira Katz, Richard R. Hofer, and Dan M. Goebel

*Jet Propulsion Laboratory, California Institute of Technology, Pasadena, California 91109, USA*

(Received 4 August 2012; accepted 20 December 2012; published online 17 January 2013)

We demonstrate by numerical simulations and experiments that the unmagnetized ion beam formed in a Hall thruster can be controlled by an applied magnetic field in a manner that reduces by 2–3 orders of magnitude deleterious ion bombardment of the containing walls. The suppression of wall erosion in Hall thrusters to such low levels has remained elusive for decades. © 2013 American Institute of Physics. [<http://dx.doi.org/10.1063/1.4776192>]

Erosion of the acceleration channel in Hall thrusters can expose its magnetic circuit to bombardment by beam ions, which can lead to the failure of the engine. By contrast to gridded thrusters, in which the ion beam can be controlled well with the proper arrangement of the electrode apertures, in grid-less arrangements like the Hall thruster focusing of the high-energy unmagnetized ions away from the discharge chamber walls is significantly more challenging because the total electric field  $\mathbf{E}$  in the inhomogeneous plasma must conform to the generalized Ohm's law. The implication is that a component of  $\mathbf{E}$  along the applied magnetic field  $\mathbf{B}$  can (and usually is) established that accelerates some beam ions towards the walls. Though unconventional electrode arrangements can indeed alter the relevant plasma properties,<sup>1</sup> no arrangement has been found that allows for sufficient control of the electric field to eliminate erosion. Consequently, since their inception over fifty years ago,<sup>2,3</sup> Hall thrusters have not been used in deep-space missions despite their enabling propulsive capabilities.

A schematic illustrating the basic features of a typical Hall thruster is shown in Fig. 1(a). The beam is produced by the formation of an azimuthal electron current that interacts with an applied quasi-radial  $\mathbf{B}$  to produce a largely axial force on the ions.  $\mathbf{B}$  is produced by a magnetic circuit such that the radius of gyration,  $R = m|\mathbf{u} \times \mathbf{B}|/qB^2$ , for electrons (e) and ions (i) obeys  $\bar{r}_e \ll 1 \ll \bar{r}_i$ , where  $\bar{r} \equiv R/L_c$ .  $L_c$  is a characteristic size for the “acceleration channel” taken here to be its length, and  $m$ ,  $q$ , and  $\mathbf{u}$  are the mass, charge, and particle drift velocity, respectively. Electrons are supplied to the channel by an electron source and diffuse to the anode across field lines by classical and (arguably) non-classical mechanisms,<sup>4</sup> while interacting with the dielectric walls through a sheath.<sup>5</sup> Ions are produced mostly by electron-impact ionization of propellant atoms. The propellant is injected typically through the anode. The electron number density ( $n_e$ ) is low enough that collisions in the azimuthal direction seldom impede their  $\mathbf{E} \times \mathbf{B}$  drift, inducing a Hall current. Operation under these conditions implies a high Hall parameter for the electrons,  $\Omega_e \equiv \omega_{ce}/\nu_e \gg 1$ , where  $\omega_{ce}$  and  $\nu_e$  are the electron cyclotron and total collision frequencies, respectively; for ions  $\Omega_i$  remains  $\ll 1$ . As the Hall current crosses  $\mathbf{B}$ , the induced  $\mathbf{E}$  is

in the direction perpendicular ( $\perp$ ) to  $\mathbf{B}$  and proportional to  $\sim \eta \Omega_e^2 \mathbf{j}_{e\perp}$  according to Ohm's law, where the electron current density and resistivity are denoted by  $\mathbf{j}_e$  and  $\eta$ , respectively.  $\mathbf{E}_\perp/q_i$  serves as the main force on the ions. Also,  $\partial \mathbf{B}/\partial t = 0$  thus  $\mathbf{E} = -\nabla \phi$ , where  $\phi$  denotes the plasma potential. The increased resistive heating of electrons in the region of high  $\mathbf{E}$  leads also to an increase in the electron temperature ( $T_e$ ). Typical  $\phi$  and  $T_e$  profiles along the channel centerline are shown in Fig. 1(b). Under these discharge conditions the resistance to the electron transport of heat and mass parallel ( $\parallel$ ) to  $\mathbf{B}$  is much smaller (by  $\sim \Omega_e^2$ ) than that in the  $\perp$  direction. Thus,  $T_e$  is approximately constant along lines of force

$$\nabla_{\parallel} T_e \approx 0. \quad (1)$$

Also, the electron momentum equation simplifies to

$$\mathbf{E}_{\parallel} \approx -T_e \nabla_{\parallel} \ln(n_e). \quad (2)$$

Equations (1) and (2) yield two known conditions along lines of force in these discharges:  $T_e \approx T_{e0}$  and  $\phi \approx \phi_0 + T_{e0} \ln(n_e/n_{e0})$ , where  $T_{e0}$ ,  $\phi_0$ , and  $n_{e0}$  are constants of integration.<sup>2</sup> Hence, though each line is nearly isothermal it is not also equipotential, which has important implications on our ability to control erosion.

Erosion of the acceleration channel walls in Hall thrusters occurs when ions bombard them with sufficient energy to sputter off material. The erosion rate is proportional to the product of the incident ion flux and the sputtering yield of the material. The latter is a strong function of the total ion energy, which consists of energy gains made in the plasma and those made inside the sheath. Henceforth, we shall use the terms “kinetic” and “sheath” to distinguish between the two energy contributions. For dielectric materials the potential fall in the sheath is dependent on  $T_e$  as derived by Hobbs and Wesson.<sup>6</sup> In such sheaths higher  $T_e$  typically implies higher sheath fall and, therefore, higher ion energy.

A set of representative  $\mathbf{B}$ -lines in a typical Hall thruster channel are illustrated in Fig. 1(b). In this configuration the variation of  $\phi$  and  $T_e$  along the walls is similar to that along the centerline because the lines are nearly radial. Consequently, the elevated  $\mathbf{E}_{\parallel}$  and  $T_e$  there can drive a flux of high-energy ions towards the walls leading to erosion of the material. For reasons that will become apparent shortly we shall designate this as the “unshielded” (US) configuration.

<sup>a)</sup> Author to whom correspondence should be addressed. Electronic mail: [Ioannis.G.Mikellides@jpl.nasa.gov](mailto:Ioannis.G.Mikellides@jpl.nasa.gov).

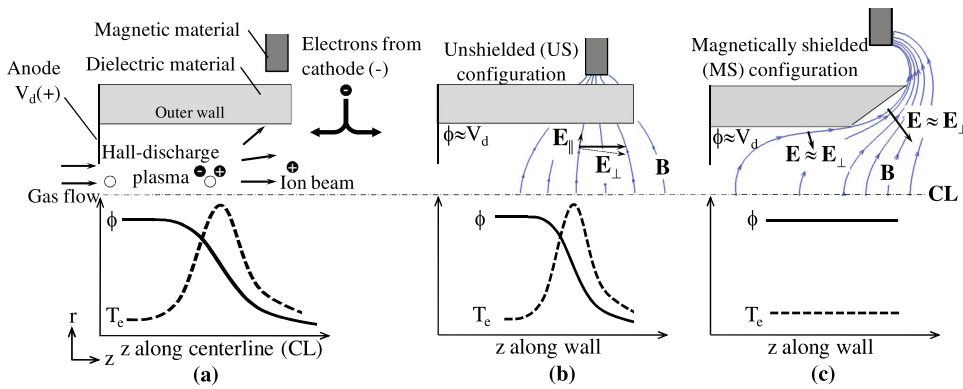


FIG. 1. Schematics of the upper half of the annular channel containing a Hall discharge (top) and typical profiles of  $\phi$  and  $T_e$  (bottom) established during ion acceleration. (a) Basic features of the accelerator and typical profiles along the centerline. (b)  $\mathbf{B}$  lines and profiles along the wall in an US configuration. (c)  $\mathbf{B}$  lines and profiles along the wall in a MS configuration.

In recent work we derived the theoretical basis of a technique termed magnetic shielding<sup>7</sup> that, in principle, eliminates wall erosion in Hall thrusters. In this article we report on the demonstration of the technique's first principles. Referring to Fig. 1(c), the fundamental premise of magnetic shielding is that  $\mathbf{B}$  may be applied in a way that sustains at the walls plasma conditions that are near the discharge extrema for  $\phi$  and  $T_e$ , namely:  $\phi \sim$  discharge voltage  $V_d$  and,  $T_e \sim$  coldest value inside the channel (which typically occurs near the anode). In this manner the incident-ion kinetic and sheath energies can be marginalized and  $\mathbf{E}$  can be controlled to be both nearly perpendicular to the surface and large in magnitude, as shown in Fig. 1(c). Such topology would force ion acceleration away from walls thereby reducing the wall-incident ion flux without loss of propulsive performance. The key principle behind magnetic shielding is based on the recognition that the electron pressure (see Eq. (2)) forces  $\mathbf{E}$  and  $\mathbf{B}$  to no longer form an orthogonal set (Fig. 1(b)). Thus, a geometry of  $\mathbf{B}$ -lines with convex curvature toward the anode (first proposed by Morozov<sup>2</sup>) cannot control  $\mathbf{E}$  and, in turn, the erosion at the surfaces effectively if the near-wall lines are not also equipotential. We argue that the  $\mathbf{B}$  topology depicted in Fig. 1(c) can overcome this drawback. Equipotentiality is achieved almost exactly by this topology because it allows  $\mathbf{B}$ -lines to extend to the anode without interruption by solid surfaces. Therefore, these lines are naturally associated with values of high  $\phi_0$  and low  $T_{e0}$ , which minimize the contribution of the electron pressure  $\sim T_e \times \ln(n_e)$ . Hereafter, we shall call the thruster configuration in Fig. 1(c) magnetically shielded (MS).

The demonstration of magnetic shielding was achieved by a combination of numerical simulations and laboratory experiments. Specifically, the wall geometry and magnetic circuit of an existing thruster were modified from their original US configuration, and the thruster was then tested in a vacuum facility at its nominal operating condition of 300 V and 20 A. The modifications were guided by numerical simulations, performed using a 2-D axisymmetric code called Hall2De. The code solves the time-dependent conservation laws for all species in the discharge on a computational mesh that is aligned with  $\mathbf{B}$ .<sup>8,9</sup> Sixteen different diagnostics were deployed during the experiments. Here, we discuss the results from cylindrical Langmuir and emissive probes, used to measure plasma properties along the channel centerline and dielectric walls. For the centerline data a fast-moving probe system was deployed to scan the near-field and interior regions of the accelerator. Flush-mounted probes at the walls were used to measure the plasma

properties along the surfaces. Also, profilometry was performed using a coordinate measuring machine (CMM), and a quartz crystal microbalance (QCM) was mounted adjacent to the device to measure the deposition rate of back-sputtered carbon.

Contour plots of the plasma properties from the numerical simulations are compared in Fig. 2. Results that are pertinent to wall erosion are plotted in Fig. 3. The effect of magnetic shielding on  $\phi$  is immediately evident in Figs. 2(a) and 2(b). Specifically, along the MS diverging wall we compute only a 4–15 V reduction compared to a drop as high as 230 V at the US inner wall near the channel exit. The kinetic energy of ions entering the sheath was, therefore, lowered by at least  $\sim 6$  times in the MS configuration as shown in Fig. 3(a).

In the last  $\sim 20\%$  of the channel we also compute a reduction in the sheath energy of about 4–10 times that in the US configuration (Fig. 3(b)). Indeed the comparison of the two configurations in Figs. 2(b) and 2(c) shows a significant reduction of  $T_e$  along these regions of the wall, which explains the decrease of the sheath fall.  $T_e$  is lowered because the  $\mathbf{B}$ -lines only graze the corner formed by the cylindrical and diverging sections of the MS channel. These lines, therefore, carry cold electrons because they extend deep into the acceleration channel (Fig. 1).

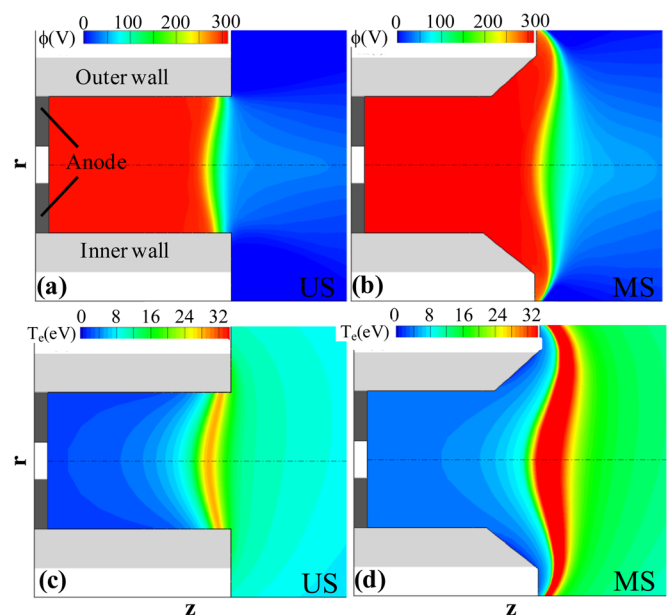


FIG. 2. 2-D axisymmetric simulations of the Hall-discharge plasma in the US ((a) and (c)) and MS ((b) and (d)) accelerator configurations.

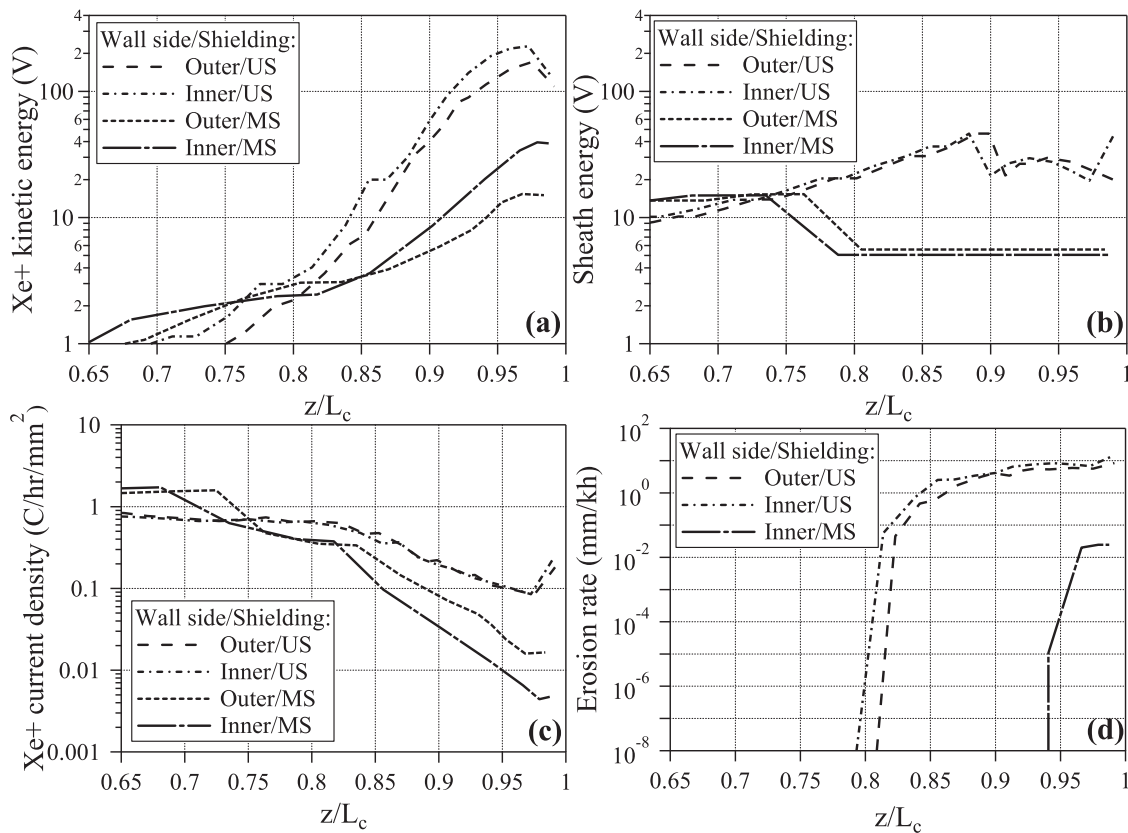


FIG. 3. Numerical simulation results along the acceleration channel walls. (a) Impact kinetic energy of  $Xe^+$ . (b) Sheath energy of  $Xe^+$ . (c) Current density of incident  $Xe^+$ . (d) Total erosion rate (accounting for three charge states of  $Xe$ ). The total ion energy at the MS outer wall is below the assumed threshold (25 V) for sputtering and thus no erosion is computed.

Finally, because near the MS walls the component of  $\mathbf{E}$  parallel to them is nearly eliminated, ion acceleration occurs largely away from the walls, which leads also to lower wall-incident ion flux. Specifically, referring to Fig. 3(c), the incident current density of singly charged ions ( $Xe^+$ ) near the channel corners was determined to be 8–50 times lower in the MS configuration. In regions where the MS fluxes are comparable to the US fluxes, it was found that the ion energy was not sufficient to cause any detectable erosion. In these calculations the dependence of the sputtering yield on the ion energy was based on the model by Bohdansky<sup>10</sup> for the same boron nitride (BN) wall material used in the experiments, and the threshold ion energy was assumed to be 25 V. Overall, we

computed more than  $\sim 600$  times lower erosion rate at the MS inner wall (Fig. 3(d)). The outer wall experienced zero erosion since the impact ion energy was found to be  $< 25$  V.

A wide range of comparisons between simulations and measurements were performed to verify the theoretical predictions, a representative set of which is presented in Figs. 4 and 5. In Fig. 4 we compare simulations with probe measurements along the channel centerline. We note here that to reduce the spatial uncertainty associated with the fast-moving probes, the axial location of the centerline data was determined based on the location of the wall probe data and the measured  $\mathbf{B}$ . This was made possible after confirming by direct measurement that the lines of force were indeed isothermal.

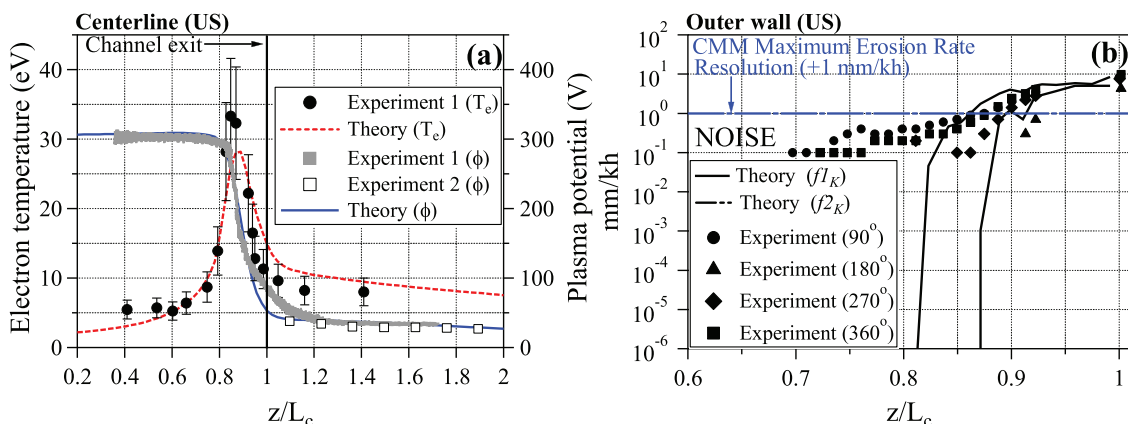


FIG. 4. Comparisons between simulations and measurements in the US configuration. (a)  $\phi$  and  $T_e$  along the channel centerline. (b) Net erosion rate along the inner wall. The measurements were obtained at four different azimuths along the channel circumference.

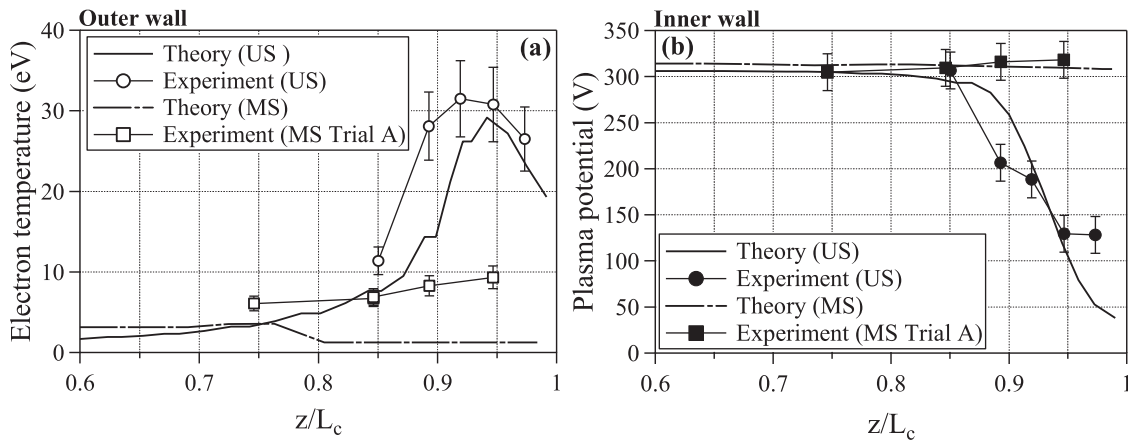


FIG. 5. Comparisons between simulations and measurements along the walls in the US and MS configurations.

Profilometry also was performed to determine the net erosion rate at the walls. These measurements are compared in Fig. 4(a) with simulation results for two sputtering yield models,  $fI_K$  and  $f2_K$ , corresponding to ion energy thresholds of 25 V and 50 V, respectively. It is noted that the simulations did not account for back-sputtered carbon from the facility and re-deposition of BN onto the walls. Referring to Fig. 4(b), it is also noted that due to the low resolution of the CMM those measured erosion rates that are below 1 mm/kh were considered ambiguous since they were within the noise level of the instrument.

Simulated and measured values of  $T_e$  at the outer wall and  $\phi$  at the inner wall are compared in Figs. 5(a) and 5(b), respectively. The comparison confirms the predicted effect of magnetic shielding along the walls. Specifically,  $\phi$  is found to be nearly constant along the MS walls by contrast to a decrease in the US configuration that exceeds 150 V. The observed trends in  $T_e$  are found also to be in general agreement with the theoretical predictions. It is worthwhile noting that after measuring **B** we found that the designed topology used in all the simulations was not reproduced precisely in the first thruster test termed here "Trial A." Spatial differences in the order of  $\sim 0.05L_c$  were detected, which are of the order of some of the discrepancies depicted in Fig. 5(a) between theory and experiment. A second test called "Trial B" that attempted to correct these minor errors was performed several months later.

Though no plasma measurements were performed in Trial B, noticeable differences between the carbon deposits at the walls were indeed observed.

Because the original color of the wall material is white carbon deposition was clearly visible upon the completion of the experiments. In the US configuration  $\sim 87\%$  of the walls were fully coated with carbon whereas in the last  $\sim 13\%$ , where the CMM showed detectable erosion (Fig. 4(b)), the material remained white. The extent of this "erosion band" is consistent also with the profiles of Fig. 5, which illustrate that ions indeed acquire significant energy in this region. In the Trial-A tests 100% and 97% of the MS outer and inner walls, respectively, were fully coated with carbon whereas the last  $\sim 3\%$  of the inner wall was only partially discolored by the carbon deposits. In Trial B the inner wall was found to be completely coated with carbon.

Without knowledge of the effective sputtering yield of BN with C-deposits the QCM measurement of the carbon deposition rate alone cannot provide a minimum of the erosion rate reduction. However, we can deduce that if the erosion and deposition rates were equal this reduction would have exceeded 3 orders of magnitude at both walls. Based solely on the wall probe plasma data and a sputtering yield model that was intermediate to  $fI_K$  and  $f2_K$  (with energy threshold of 30.5 V), the erosion rate was found to be at least  $\sim 1000$  times ( $\pm 60\%$ ) lower at the MS inner wall. At the

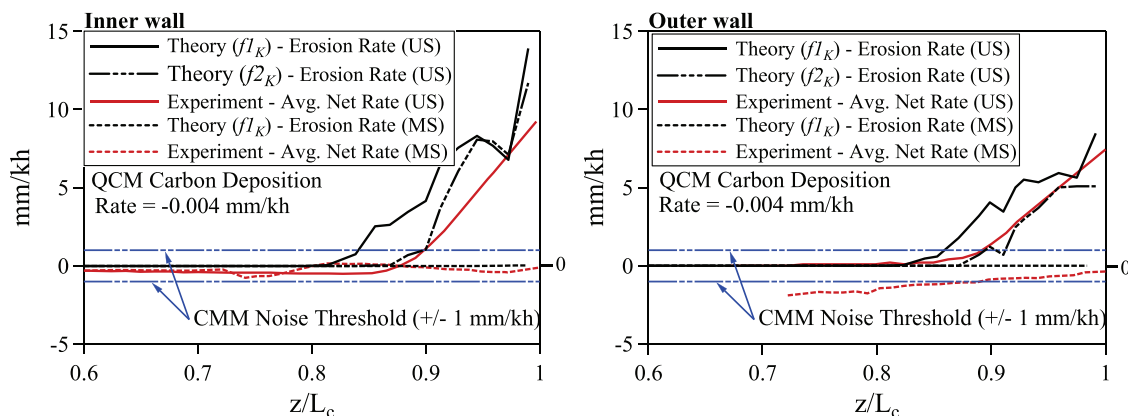


FIG. 6. Comparisons of the rates of material removal/deposition along the inner (a) and outer (b) channel walls in the US and MS configurations. The simulation results for the US configuration are given for two sputtering yield models with energy thresholds of 25 V ( $fI_K$ ) and 50 V ( $f2_K$ ). Only  $fI_K$  yields a non-zero erosion rate at the inner wall of the MS configuration; at the outer wall the ion energy is below the threshold. The CMM data are net average rates.

outer wall the ion energy was below the threshold. This is consistent with the simulations, which predict a reduction of  $\sim 600$  times at the MS inner wall and ion energies below the threshold at the outer wall. In Fig. 6 erosion rates from the simulations are compared with net rates measured by the CMM, averaged over the four circumferential locations shown in Fig. 4(b). The measurements in Fig. 6 were obtained after the thruster configurations were operated for  $>19$  h. Also depicted on these plots are the CMM noise threshold limits ( $\pm 1$  mm/kh) and the carbon deposition rate ( $-0.004 \pm 0.001$  mm/kh) measured by the QCM. Negative and positive values on these plots indicate net deposition and net erosion, respectively.

Collectively, the results from the numerical simulations and the experiments point consistently to the conclusion that the erosion was reduced in the MS configuration by at least 2–3 orders of magnitude. The finding is significant because such reductions of the wall erosion in Hall thrusters solves a problem that has remained unsettled for more than five decades, allowing for deep-space exploration missions that could not be undertaken in the past.

This research was carried out at the Jet Propulsion Laboratory (JPL), California Institute of Technology, under a contract with the National Aeronautics and Space Administration and funded by the JPL Research and Technology Development program. The authors are grateful to Al Owens and Ray Swindlehurst for assisting with the experiments in the Owens vacuum chamber at JPL.

<sup>1</sup>Y. Raitses, M. Keidar, D. Staack, and N. J. Fisch, *J. Appl. Phys.* **92**(9), 4906–4911 (2002).

<sup>2</sup>A. I. Morozov and V. V. Savelyev, in *Reviews of Plasma Physics*, edited by B. B. Kadomtsev and V. D. Shafranov (Consultants Bureau, New York, 2000), Vol. 21, pp. 203–390.

<sup>3</sup>A. I. Morozov, *Plasma Phys. Rep.* **29**(3), 235–250 (2003).

<sup>4</sup>N. B. Meezan, W. A. Hargus, and M. A. Cappelli, *Phys. Rev. E* **63**(2), 026410 (2001).

<sup>5</sup>D. Sydorenko, I. Kaganovich, Y. Raitses, and A. Smolyakov, *Phys. Rev. Lett.* **103**(14), 145004 (2009).

<sup>6</sup>G. D. Hobbs and J. A. Wesson, *Plasma Phys.* **9**(1), 85–87 (1967).

<sup>7</sup>I. G. Mikellides, I. Katz, R. R. Hofer, D. M. Goebel, K. de Grys, and A. Mathers, *Phys. Plasmas* **18**(3), 033501 (2011).

<sup>8</sup>I. G. Mikellides and I. Katz, *Phys. Rev. E* **86**(4), 046703 (2012).

<sup>9</sup>I. Katz and I. G. Mikellides, *J. Comput. Phys.* **230**(4), 1454–1464 (2011).

<sup>10</sup>J. Bohdansky, *Nucl. Instrum. Methods B* **2**(1–3), 587–591 (1984).